Reducing Substrate Pinning of Block Copolymer Microdomains with a Buffer Layer of Polymer Brushes

Christopher Harrison,* Paul M. Chaikin, and David A. Huse

Department of Physics, Princeton University, Princeton, New Jersey 08544

Richard A. Register

Department of Chemical Engineering, Princeton University, Princeton, New Jersey 08544

Douglas H. Adamson and Abishai Daniel[†]

Princeton Materials Institute, Princeton University, Princeton, New Jersey 08544

E. Huang, P. Mansky,[‡] and T. P. Russell

Polymer Science and Engineering Department, Silvio O. Conte National Center for Polymer Research, University of Massachusetts, Amherst, Massachusetts 01003

Craig J. Hawker

IBM Almaden Research Center, 650 Harry Road, San Jose, California 95120-6099

David A. Egolf, Ilarion V. Melnikov, and Eberhard Bodenschatz

Laboratory of Atomic and Solid State Physics, Cornell University, Ithaca, New York 14853-2501

Received September 13, 1999; Revised Manuscript Received November 16, 1999

ABSTRACT: We study the range of orientational order of a single layer of cylindrical block copolymer microdomains annealed on several types of substrates. The orientational persistence length or nematic correlation length (ξ) is evaluated using recently developed imaging and analysis methods to measure the grain size of the block copolymer microdomains. We show that the substrate can lower ξ for block copolymers with a majority component that interacts strongly with the substrate, but this can be mitigated by attaching a buffer layer of polystyrene brushes to the substrate. In addition, we show that, for a block copolymer where the block that strongly interacts with the substrate is the minority component, the microdomain correlation length does not increase when substrates are treated with this buffer layer. We suggest that in this case the brushes do not increase ξ not only because of the lower volume fraction of the strongly interacting component but also because there are block copolymer wetting layers at the free and substrate interfaces that decouple the microdomains from the substrate in a similar manner as the polystyrene brushes.

Introduction

Block copolymers are amphiphilic molecules consisting of two or more components which microphase separate in the melt. Connectivity constraints force microphase separated blocks to share the same interface, producing the familiar morphologies of lamellae, gyroid, cylinders, or spheres depending on the volume fraction of the components.[1] Though well studied for several decades in the bulk, these morphologies have recently been the focus of much research in thin films.[2] The thickness of the film is chosen such that the number of microdomain layers is typically of order unity. In addition, the film is usually enriched in one block at the vacuum interface and at the substrate interface; the composition of these two "wetting layers" may be the same or different, according to which block has the greatest affinity for each interface. By effectively lowering the number of dimensions to two, the microdomains become simpler to image and the physics becomes simpler to elucidate.

Though copolymer microdomain morphologies have been well examined, the microdomain correlation length ξ—a measure of the local degree of order in the system or a measure of "grain size"—has been investigated by remarkably few studies. The work of Balsara and coworkers, a notable exception, has established the utility of birefringence and depolarized light scattering for examining the kinetics of the growth of grains.[3−7] The grain size is ξ^d, where d is the dimension of the system. However, Balsara's research focused on bulk samples ($d = 3$), and there has been a paucity of studies relating to the development of microdomain correlation length in thin films supported by substrates. Understanding and controlling the microdomain ordering is paramount to the effective use of these layers as lithographic templates.[8,9]

The largest impediment to studying this problem has been the difficulty of reliably obtaining high-quality microdomain images, but recent developments have eliminated this problem. Past researchers have relied heavily upon the complementary techniques of transmission electron microscopy with selective staining to

* To whom correspondence should be addressed.
[†] Current address: Applied Physics Department, University of Michigan, 2477 Randall Laboratory Ann Arbor, MI 48109-1120.
[‡] Current address: Symyx Technologies, 3100 Central Expressway, Santa Clara, CA 95051.

10.1021/ma991551g CCC: $19.00
Published on Web 12/28/1999

examine the morphology of microdomains, but the time-consuming nature of this procedure greatly limits the number of samples studied. Atomic force microscopy has also been applied to copolymer systems with varying degrees of success.[10−12] More recently, our group has developed a technique that relies upon removal of material from the top surface of the polymer film by a reactive ion etcher and the resolution of a low-voltage scanning electron microscope to produce high-quality images.[13,14] This technique has been applied to polystyrene−polybutadiene and polystyrene−polyisoprene systems and, most recently, to polystyrene−poly(methyl methacrylate) systems.[15]

It has been suggested that the substrate plays a large role in limiting the resulting microdomain order in thin films. This effect will be strongest for polymers that can bind to the substrate. It has been observed by our group and others that polybutadiene can strongly adhere to silicon oxides such as bulk glass and the native oxide of a silicon substrate.[13,16,17] Therefore, microdomains in polybutadiene-rich copolymers should be pinned on silicon substrates, yielding a small value of ξ. This pinning has been previously observed by Mansky et al.[18] in a butadiene-rich styrene−butadiene diblock copolymer, but as we will show, substrate pinning can be overcome through appropriate modification of the substrate, such as applying a layer of polystyrene brushes to the substrate. However, for polystyrene-rich copolymers this substrate pinning effect is much smaller, both because of the lower volume fraction of polybutadiene and because the microdomains are decoupled from the substrate by wetting layers.

Experimental Section

1. Synthesis and Fractionation. A polystyrene-rich diblock copolymer was synthesized by standard high-vacuum anionic techniques in a cyclohexane/benzene (90/10 v/v) mixture to yield a high 1,4 content in the polybutadiene block.[19] This diblock copolymer (SB 36/11) was synthesized with a composition of 36 kg/mol for the polystyrene (PS) block and 11 kg/mol for the polybutadiene (PB) block such that microphase separation produces PB cylinders in a matrix of PS. The upper glass transition temperature was measured with a Perkin-Elmer differential scanning calorimeter (model DSC 7) to be 367 K. The molecular weights were determined by combining the volume fraction determined through ^{1}H NMR (model GE 300) with the molecular weight of the first synthesized block as determined by a Waters gel permeation chromatography (GPC) system equipped with three Phenogel GPC columns.

For studies involving PB-rich copolymers, Kraton D1102 was obtained from Shell Chemical (hereafter referred to as SBS). In the melt, this copolymer forms PS cylinders in a PB matrix. Molecular characterization of SBS has been reported previously;[21] the styrene blocks comprise 26 wt % of the material, which is roughly 85 wt % symmetric (SBS) triblock and 15 wt % uncoupled (SB) diblock of identical composition and half the molecular weight of the triblock. The upper glass transition temperature of this polymer, which was difficult to detect by DSC, should be approximately 340 K on the basis of the known molecular weight and composition.[20] There may also be processing oils in the as-received SBS copolymer, as well as trace homopolystyrene from the terminated first block, which could affect results.[21] Attempts to use this material as received consistently produced polymer films that dewetted the substrate without terracing. The typical terracing of block copolymer films on substrates into islands and holes after annealing was not observed. Instead, the polymer film appeared to dewet into a random pattern of dramatically varying thickness without any regularity or a dominant length scale. An essentially pure triblock fraction of SBS was isolated by standard solvent/nonsolvent fractionation.[22] Methanol was added to a 0.2% solution of SBS in toluene as the temperature of the solution was raised to nearly the boiling point of the mixture. The solution was then allowed to cool slowly, and the higher molecular weight species preferentially precipitated. The resulting fraction showed a monomodal molecular weight distribution by GPC analysis, with a polydispersity of 1.07. After this fractionation process, SBS did not dewet substrates upon annealing.

2. Surface Cleaning. Since we are interested in the effect of the substrate on the copolymer film, great attention was paid to preparing consistently clean surfaces. All surface cleaning was carried out on 3 in. silicon wafers ($\langle 1-0-0 \rangle$ orientation, Silicon Quest International) in a clean room that was class 100 or better to minimize airborne contamination. Substrate exposure to air was kept below $^1/_2$ h between preparation of the surface and application of the copolymer film. Silicon wafers that were exposed to clean room air for times longer than several hours were significantly less clean as determined by examining the contact angle of deionized (DI) water applied to substrates. DI water applied to clean wafers has a miniscule contact angle (DI water wets clean wafers), and DI water applied to contaminated wafer surfaces dewets with contact angles large enough to evaluate by eye. We found that DI water consistently wets substrates after being exposed to air for less than $^1/_2$ h, which we set as our maximum allowable time between preparation of the surface and coating with copolymer.

To clean silicon wafers, we remove the topmost layer of silica to expose a new layer underneath with the ultimate level of cleanliness. We do this by first cleaning the wafers with 10 s dips in trichloroethylene, acetone, and 2-propanol (all at ambient temperature) and blow drying the wafer with a stream of filtered nitrogen after each dip. The wafers are then dipped into buffered oxide etch (typically denoted 10:1 BOE, containing 35% (w/w) NH_4F and 4.4% (w/w) HF and surfactants) for 10 s to remove the native oxide and rinsed with deionized water. Remaining water is blown off the silicon wafer surface with a filtered nitrogen gun, and the wafer is dipped into a 70% solution of HNO_3 for no more than 10 s to reoxidize the surface, followed by a vigorous deionized water rinse, and dried with nitrogen again. The wafer surface consists of a hydrophilic oxidized layer of thickness 1−2 nm. Wafers with large-scale imperfections were rejected and discarded, though wafers with only one or two specks of microscopic dust were judged acceptable. After cleaning the wafers, care was taken to quickly coat them with copolymer.

3. Carbon Coating. To attempt to provide a substrate similar to carbon-coated TEM grids, silicon wafers were cleaned as described above and then vacuum-coated with carbon (Denton Vacuum carbon coater, model DV-502). One inch of carbon embedded thread was placed between two electrodes through which current flowed for 5 s, heating the carbon thread to a glowing white and coating the wafers with approximately 10 nm of carbon. Copolymer layers were subsequently spin-coated on these carbon-coated wafers.

4. PS Brush Coating. Polystyrene brushes were synthesized via TEMPO (2,2,6,6-tetramethylpiperidinyl-1-oxy) "living" free radical polymerization.[15,23−26] This produced polymers with a hydroxy terminus at one end and a TEMPO terminus at the other. The molecular weight was determined by GPC to be 9.8 kg/mol, with a polydispersity (M_w/M_n) of 1.11. The brushes were dissolved in toluene at 1% and spin-coated at 5K rpm onto wafers that were cleaned with the procedure described above. This process uniformly applied a layer approximately 5 nm thick layer to the wafer.

The film thickness was measured with either a Rudolph Research ellipsometer with a helium−neon laser ($\lambda = 633$ nm) or a Leica interferometer. The brush-coated wafers were vacuum-annealed for 12 h at 448 K to anchor the hydroxy terminus of the brushes to the native oxide of the wafers. After annealing, the wafers were dipped into toluene to dissolve away any unattached brushes, producing an extremely hydrophobic surface with a 5 nm thick layer of brushes, as measured by ellipsometry. These surfaces were then rapidly coated with copolymer.

5. Copolymer Film Preparation. Vacuum annealing was carried out in a Fisher Scientific model 280 vacuum oven that had a base pressure better than 1 mTorr when operated with an oil-based diffusion pump backed by a roughing pump. All samples were annealed for 12 h at temperatures ranging from 395 to 456 K. After annealing, samples were stained with the vapors of a 4% solution of OsO_4 (Polysciences) for at least 2 h to provide contrast for electron microscopy.

When comparing the effect of various substrates on the copolymer microdomain correlation lengths, copolymer layers were applied within a short time to all substrates after cleaning and preparation. To most accurately compare the influence of the various substrates, copolymer films on various substrates were annealed together in the vacuum oven. For example, when comparing the influence of the bare silicon substrate and the PS brush-coated substrate on the correlation length of SBS microdomains as a function of temperature, both sets of samples were prepared and annealed together.

6. Reactive Ion Etching. To image the copolymer film's internal microdomains with a scanning electron microscope, the free surface wetting layer was removed by reactive ion etching. Polymer film etching was performed at the Cornell Nanofabrication Facility (CNF) using a customized reactive ion etcher by Applied Materials. The etching process was performed[27] at a CF_4 flow rate of 10 standard cubic centimeters per minute (SCCM), a pressure of 2 mTorr, and a power density of approximately 0.03 W/cm^2. A dc self-bias of approximately 290 V developed between the anode and the cathode, on which the sample was placed. As we have shown previously, CF_4 RIE with the above parameters produces a nonselective and smooth etching process that allows us to adequately control the etch depth.[13] For both the SBS and SB 36/11 films, 1 min of etching removed approximately 12 nm of polymer film, exposing the internal microdomains to the surface for optimal imaging contrast.

7. Scanning Electron Microscopy. The SEM images in this paper were obtained with a Leo Gemini 982 field emission gun SEM at CNF. The resolution at 1 kV is specified as 4 nm. SEM work was performed with an incident electron beam energy between 1 and 3 kV and by collecting secondary electrons (SE) or, when available, secondary plus backscattered electrons (BSE). A higher resolution was typically seen with the combined signals as opposed to each signal independently because of the increased signal-to-noise ratio. The working distance was typically 2−4 mm in order to optimize the resolution. The regions of electron microscope images with a higher electron yield (which appear brighter in images) correspond to the osmium-stained PB regions of the sample.

The SEM images were typically obtained at a magnification of 30 000 with horizontal and vertical dimensions of 3.8 and 2.93 μm, respectively, for a total area of 11.13 μm^2. With a 1024 pixel horizontal extent, this translated to 3.71 nm/pixel, approximately the resolution limit of the instrument. The chosen magnification was a compromise between the need to image many grains of microdomains per image while maintaining a distance of at least 6 pixels between microdomains, the minimum distance necessary for robust calculation of the local orientation. For samples with shorter correlation lengths, some images were obtained at a magnification of 50 000, which had horizontal and vertical dimensions of 2.28 and 1.76 μm, respectively.

Results and Discussion

1. Ascertaining the Appropriate Film Thickness for a Single Layer of Microdomains. Each type of substrate described above has different boundary conditions at its interface with the copolymer film. It has been shown with dynamic secondary ion mass spectrometry (SIMS) that, for silicon substrates with a native oxide, the PB component of a PS−PB copolymer wets the substrate.[13] In addition, PB wets the free surface as it is the lower surface tension component (Figure 1a). For the polystyrene-rich SB 36/11, therefore, the polydiene component wets both the free and confined surfaces, requiring approximately 50 nm of polymer film to produce one layer of microdomains sandwiched between the top and bottom layers. A 50 nm thick film is produced by spin-coating a 1.5% solution at approximately 3K rpm. This appropriate thickness was determined by a combination of TEM, SEM, ellipsometry, and optical measurements. A similar thickness of the copolymer film was observed to be necessary to produce one layer of microdomains on carbon-coated wafers, indicating that polybutadiene wets the carbon substrates as well.

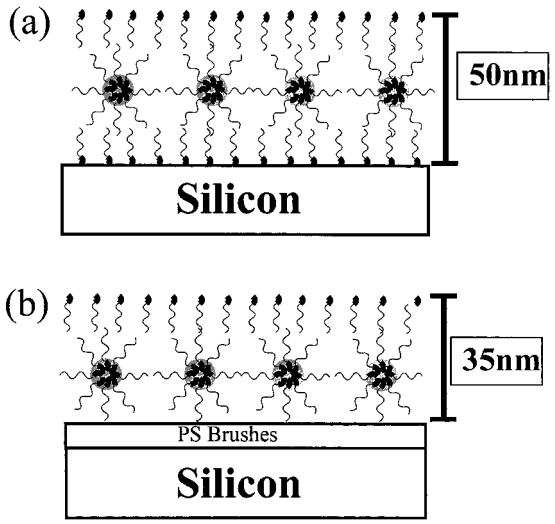

Figure 1. Idealized polymer chain configuration within one layer of SB 36/11 microdomains on two types of substrates. The heavier lines represent the polybutadiene block and the lighter lines the polystyrene. This schematic has been established through dynamic secondary ion mass spectrometry. (a) Silicon wafer with with native oxide. Note the wetting of the free and confined surfaces with additional polymer chain layers. The total thickness is 50 nm. (b) Silicon wafer with PS brushes. Note that the PS blocks of the copolymer wet the PS brushes. With the absence of the additional wetting layer seen in (a), the copolymer film thickness is only 35 nm.

However, by attaching a layer of PS brushes to the substrate, we change the substrate wetting conditions, inducing the PS component of the SB 36/11 copolymer to wet the PS molecules of the brush. Eliminating the need to wet the substrate with an additional polydiene layer reduces the thickness of the polymer film necessary to produce one layer of microdomains (see Figure 1b). This schematic has been well supported through dynamic SIMS data on poly(methyl methacrylate)-coated wafers, which are also preferentially wet by the PS component of PS−PB copolymers.[28] For example, it was observed through ellipsometry that 50 nm of polymer film was required to form a monolayer of SB 36/11 microdomains on a silicon substrate, but only 35 nm (spun from a 1% solution at 3K rpm) was required to form a monolayer of microdomains on a PS brush-coated substrate. Note that these thicknesses do not include the approximately 5 nm thick PS brush layer.

The silicon wafer's surface properties affected thin films of SBS in a surprisingly different manner. As annealed on the bare wafer, the SBS copolymer did not produce the typical terracing of islands and holes, even for a wide range of sample thicknesses (30−100 nm). We suspect that the strong interaction of the substrate with the polybutadiene pins the polymer chains, inhibiting the diffusion necessary to produce terracing. Inves-

tigations with electron microscopy revealed that these films produced microdomains with very short correlation lengths, comparable to the microdomain periodicity, as will be shown below. SBS films annealed on carbon-coated or PS brush-coated wafers, however, showed the typical terracing of copolymer films with significantly longer correlation lengths. This terracing is easily observed via optical microscopy by the interference colors produced by, for example, regions with thicknesses of one or two layers of microdomains. Surprisingly, for both the PS brush-coated and carbon-coated substrates, a monolayer of SBS microdomains was observed for a thickness of approximately 45 nm, produced by spin-coating a 1% solution at 4K rpm. Though we would expect a different microstructure for these two monolayers due to the different copolymer affinities of the two substrates, the similar thickness of these monolayers suggests that the polybutadiene component of SBS wets both the carbon coating and the PS brush layers, perhaps due to the slight permeability of the brushes.

Having determined that substrates coated with PS brushes allowed SBS microdomains to more closely approach their equilibrium configuration, we confirmed that spin-coating at thicknesses greater or less than this monolayer thickness caused the usual production of islands or holes on these substrates.[29] Ultrathin layers of SBS spin-coated at 20 nm on PS brush-coated wafers produced a "zeroth" layer of SBS which was of uniform thickness after annealing. SEM images of SBS films were obtained as described previously, with OsO_4 staining and imaging both unetched samples and samples that had had 15 nm of the polymer at the free surface etched away. Attempting to image copolymer microdomains at 1 kV without etching away the PB wetting layer typically produced low (or no) contrast images as the PS cylinders are submerged inside the PB matrix. There were no microdomains observed by SEM in this zeroth layer, consistent with previous work on the zeroth layer of microdomains (Figure 2a).[13] The actual morphology of this zeroth layer has not yet been examined: it could consist of the PS component of the SBS wetting the PS brushes and PB on the free surface or a PS layer between layers of PB. Spin-coating a slightly thicker film produced the typical islands of microphase-separated structures on a background of the zeroth layer (Figure 2b). The thickness of the islands was measured by interferometry to be 45−50 nm thick. Spin-coating at a thickness of approximately 45 nm produced a uniform monolayer of cylindrical microdomains, as shown in Figure 3.

For both thin films of SB 36/11 and SBS we attempted to produce the optimum thickness for a microdomain monolayer, as excess or insufficient copolymer produced islands or holes. Though this did not seem to particularly affect ξ for the cases where the islands were much larger than ξ, this made the SEM imaging more difficult as it was necessary to find regions with a commensurate thickness.

2. Studies of ξ for SBS Copolymer. A. Example of Correlation Length Measurement. We studied the influence of substrate−copolymer interaction on the microdomain correlation length of fractionated SBS. This readily available triblock copolymer forms PS cylinders in a PB matrix and has been the focus of much work in the block copolymer community.[30,31] Two representative SEM images of the microdomain patterns after annealing for 12 h at 411 K are shown in Figure 3. Note that only small portions of the entire SEM images are shown in Figure 3 for clarity. The microdomains annealed on the bare silicon wafer (Figure 3a) show a pattern with a short persistence or correlation length as compared to the microdomains annealed on the PS brush-coated silicon wafer (Figure 3b).

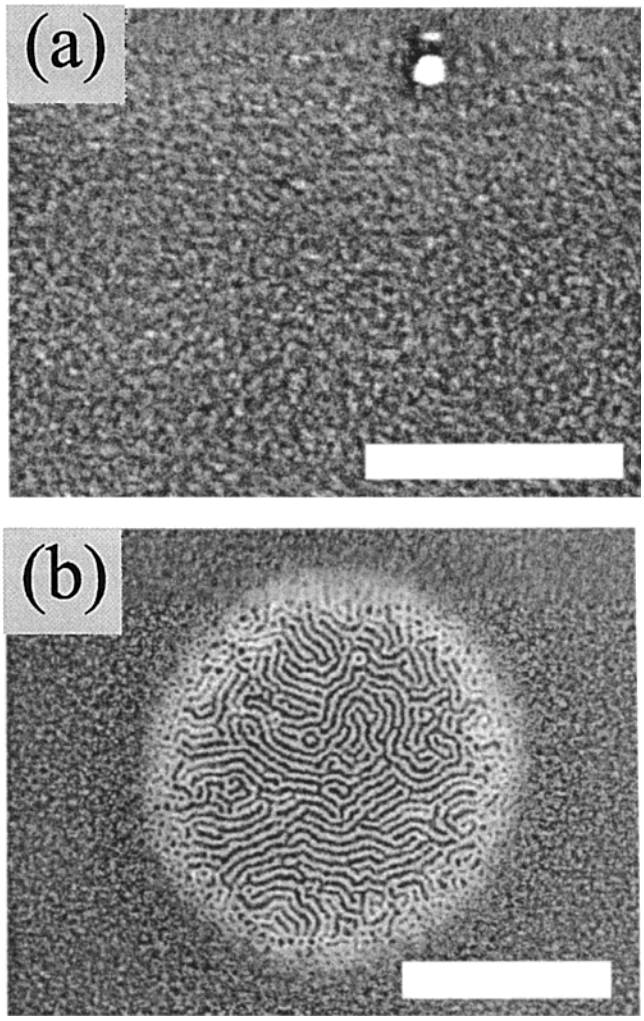

Figure 2. Two representative SEM images of SBS films of increasing thickness on PS brush-coated wafers. (a) A 20 nm thick film produces a uniform layer without terracing. The actual morphology most likely consists of wetting layers without microdomains, referred to as the zeroth layer. The light circular dot at the top of the image is a 40 nm wide gold colloidal particle that was used for aligning the electron microscope. Bar = 400 nm. (b) Spin-coating and annealing a slightly thicker film produces isolated islands of microdomains. The thickness of the islands is approximately 45 ± 5 nm. Bar = 400 nm.

A calculation of ξ was performed for both of the images of Figure 3 as will be described in detail below. The order parameter was first calculated at each point in the image using the subsequently described computational analysis (including Fourier filtering, as in Figure 4). The correlation functions of the orientational (or nematic) order parameter ($g_2(r) = \langle e^{2i\theta(0)}e^{-2i\theta(r)}\rangle$, where the brackets imply an azimuthal average) were then calculated and are plotted in Figure 5. Note that $g_2(r)$ decreases in a roughly exponential fashion more rapidly with position for the SBS film on a bare silicon wafer than $g_2(r)$ for the SBS film on the PS brush-coated wafer. Observing the roughly exponential decay, we set $g_2(r) = e^{-r/\xi}$ and find ξ from the condition that $g_2(\xi) =$

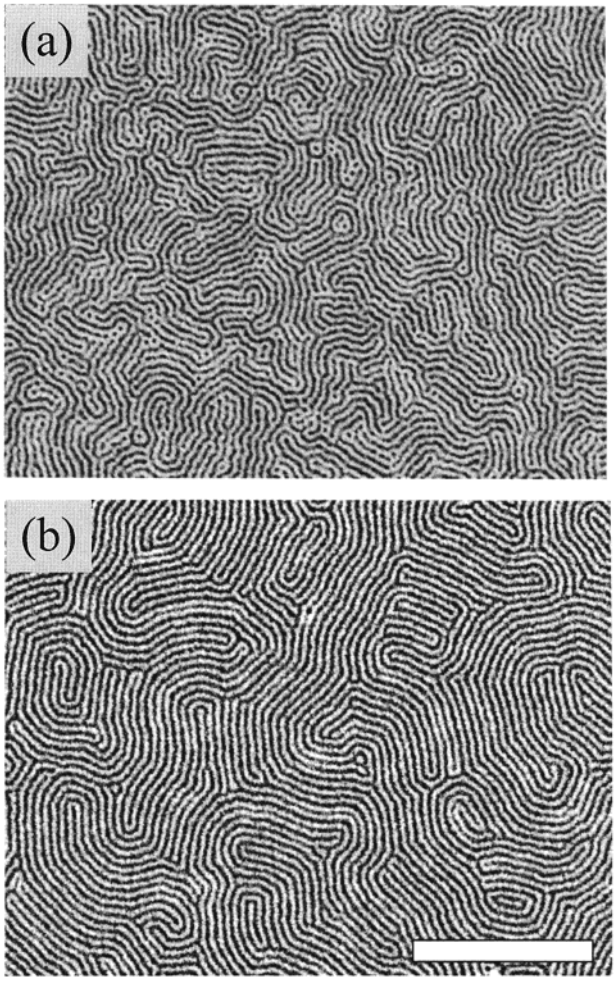

Figure 3. Two representative SEM images of SBS annealed for 12 h at 411 K on a bare silicon wafer and a PS brush-coated wafer. (a) On the bare silicon wafer, the polymers are pinned, limiting the value of ξ to 74 nm. (b) On the PS brush-coated wafer, the polymers are less pinned and produce a structure closer to equilibrium with $\xi = 122$ nm. Note also the correspondingly smaller density of defects. Bar = 400 nm.

e^{-1}. ξ for the SBS microdomains on the silicon wafer is 74 nm ($\approx 3\lambda$, where λ is the microdomain spacing of 25 nm), and ξ for the SBS microdomains on the PS brush-coated wafer is 122 nm ($\approx 5\lambda$), indicating that the PS brush-coated surface allows the microdomains to more closely approach their equilibrium configuration.

B. Description of Correlation Length Calculations. a. Introduction. Since the SEM images obtained with the Leo 982 are stored in standard 8-bit gray scale tagged image file format (TIFF), they can be directly imported into a PC-clone environment and computationally analyzed. In this section we will describe both the physical significance of the patterns observed in the images and the computational techniques used to analyze these patterns. Most of these techniques involve the implementation of physical concepts into straightforward computer programs.[32] We note that analogous methods have been employed by Garetz, Balsara, and co-workers to analyze lamellar microdomain patterns.[5]

b. Orientational Order Parameter for Microdomains. Diblock copolymers that are microphase-separated into lamellae are classified as smectic A_2 liquid crystals due to their translational and rotational symmetries.[33,34] The role of the mass density in classical smectic A systems is provided by the modulation in the two block densities through adjacent lamellae. These systems are denoted A_2 since the layer repeat spacing occurs over a distance corresponding to the radii of gyration of two molecules (Figure 6). Amundson and co-workers, among others, have investigated the validity of this treatment and calculated the elastic constants for splay and layer compressibility for smectic copolymers.[35]

Single layers of cylinders on a substrate, such as are the focus of this paper, have the same broken symmetry and order parameter as a two-dimensional smectic liquid crystal (Figure 6).[36] They are characterized by a local periodicity and local director perpendicular to the cylinders. Whereas the single layer of cylinder microdomains consisting of diblock copolymers will be treated as a two-dimensional smectic A_2, as described above, the single cylinder microdomain consisting of triblock copolymers will be denoted as smectic A since one triblock copolymer can span the entire repeat spacing. Since the distortion energy of the cylinders in both cases can then be approximated from the formalism of smectic liquid crystals, we will briefly review the relevant distortions and their energies here. Twist is intrinsically a three-dimensional effect and hence does not play a role here. Molecular bend requires nonuniform layer spacing and is less likely to occur than the formation of dislocations. Molecular splay[35] can be produced with a constant layer spacing and occurs with an energy density proportional to $1/R_c^2$ where R_c is the radius of curvature of the microdomains.

As the data will show, a similar order parameter as used for studying nematic liquid crystals is quite effective in analyzing orientational order in block copolymer microdomain patterns. Though microphase separated copolymers are *not* nematic, the nematic order parameter is more useful here as it better characterizes the orientational order of the cylinders. It is the variation in orientation of the cylinders that controls the order in our system. Translational order—measured from the width of the dominant Fourier peak—is more useful for systems that are better ordered, i.e., have a much lower density of disclinations and dislocations. In future papers we will compare correlation lengths calculated with both orientational and translational order parameters.

The local order parameter, $\psi(\vec{r})$, for nematic systems in two dimensions can be written as

$$\psi(\vec{r}) = \exp[2i\theta(\vec{r})] \tag{1}$$

where θ is the local angle of the nematogen. A factor of 2 is included in the argument of the exponent as the orientation of a nematogen is 2-fold degenerate; the molecules are symmetric. In the case of microdomains, θ will be the angle presented by the microdomains (perpendicular to the cylinder axis), and we will refer to ψ as the orientational order parameter. Again, a factor of 2 is included as the orientation of the cylinder is also 2-fold degenerate.

We note that in three dimensions the cylinder axis orientation is 2-fold degenerate whereas the orientation normal to the cylinder surface is infinitely degenerate; i.e., there are an infinite number of directions that are perpendicular to the cylinder surface. Hence, the axial orientation is better defined and generally preferred in three dimensions. However, when a cylinder is confined to a plane and can be treated as two-dimensional, both the cylinder axis direction and the direction normal to

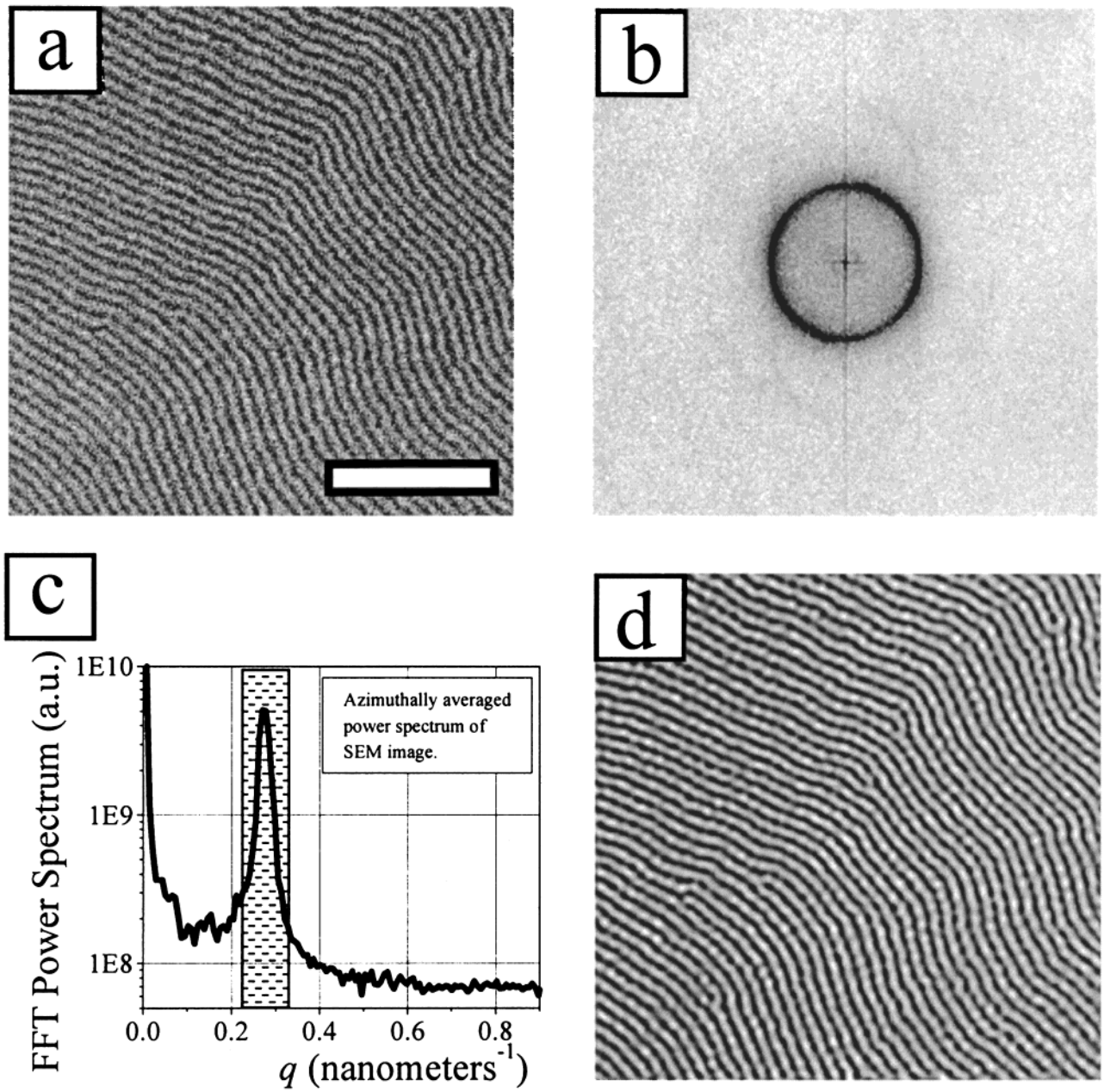

Figure 4. Fourier filtering an image. (a) SEM image of one layer of cylinders on a substrate. For clarity, only a small portion of the image is shown. High spatial frequency noise can be observed at a resolution below that of the SEM. Bar = 250 nm. (b) Power spectrum of the Fourier transform of a region much larger than (a), where the azimuthally symmetric "powder pattern" confirms that there is no preferred orientation of the cylinders when averaged over the entire image. (c) Azimuthally averaged power spectrum, showing the strongly represented cylinder repeat spacing at $q_0 = 0.25$ nm^{-1}. Only data within the shaded area, with window width roughly ±20% q_0, are inversely Fourier transformed to produce the filtered image. (d) Fourier filtered image where high-frequency noise has been removed and the contrast has been enhanced.

the cylinder surface are 2-fold degenerate and hence equally useful descriptions. As we will show, it is computationally convenient to assign the director angle to lie perpendicular instead of parallel to the cylinder axis.

c. Fourier-Filtering. Before calculating the local order parameter and resulting correlation length, all data were first Fourier-filtered by transforming to q space, and a notch filter was used to eliminate all spatial frequencies more than roughly 20% above and below q_0, the dominant microdomain frequency (Figure 4). The Fourier-space intensity at q_0 was typically at least 10 times higher than the intensities above and below q_0. This dominant frequency can be used to determine λ, the dominant repeat spacing, by the usual relation of $\lambda = 2\pi/q_0$. By eliminating frequencies significantly below q_0, low-frequency artifacts were reduced, such as typical charging effects in the top third of the image. By eliminating frequencies significantly above q_0, high-frequency noise was eliminated throughout the image. For Fourier filtering, the Image Processing Toolkit from Reindeer Games, Inc. (a standard plug-in for Adobe Photoshop) was used with Adobe Photoshop 4.0 running on an IBM-compatible personal computer (PC-clone). The calculation of the correlation length was not significantly dependent on the shape of the Fourier filter.

d. Order Parameter Calculations. To calculate the angle of the orientational order parameter, programs were written on a PC-clone that use the SEM TIFF images (whose intensity fields are denoted $I(x,y)$) to

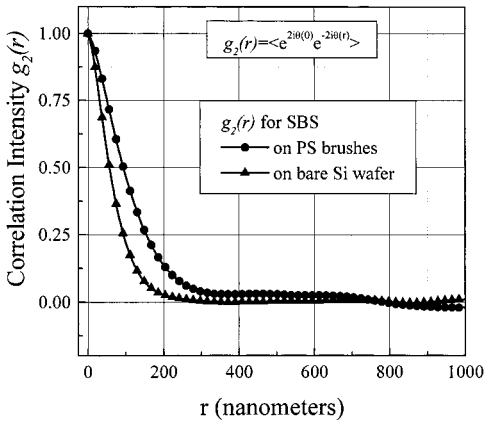

Figure 5. Orientational order parameter correlation function $g_2(r)$ for the images of SBS microdomains shown in Figure 3. The roughly exponential decay of the autocorrelation intensity $g_2(r)$ indicates short-range orientational order. We measure the correlation length from the decay of the correlation intensity $g_2(r)$ to be 74 nm for the microdomains annealed on the silicon wafer (left curve) and 122 nm for the microdomains on the PS brush-coated wafer (right curve).

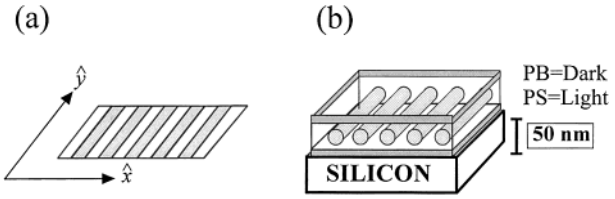

Figure 6. (a) Two-dimensional smectic liquid crystal, infinite in extent in the x and y directions, where the mass density modulations are depicted with alternating light and dark regions. (b) A single layer of diblock copolymer microdomain cylinders with the same translational and rotational symmetries as the 2D smectic of (a).

determine the local orientation of the cylinder microdomain pattern. The details of this process can be found elsewhere,[37] but a brief description will be presented here. It was first noticed that the light and dark regions occupy approximately equal areas, which, after Fourier filtering, have smoothly varying intensity modulations. Though the segregation strength of the typical polystyrene−polydiene copolymers used in this work is sufficiently high that concentration modulations through a slice of cylinders could be better approximated by a square wave, the intensity modulations of the microdomains in the SEM images appear to be sinusoidal due to a combination of the density profile of the cylinders (as observed from plan view) and the resolution limit of the SEM. Therefore, the gradient vector ($\nabla\vec{I}(x,y)$) can be used to determine the local orientation (eq 2).

$$\nabla\vec{I} = \left(\frac{\partial I}{\partial x}, \frac{\partial I}{\partial y}\right) \tag{2}$$

The orientation of the microdomain can be calculated from the local angle (ϕ) of the gradient vector. However, the gradients on either side of a PB cylinder (the cylinder is the higher intensity region) point in opposite directions, both inward. These two directions must yield the same director, which is accomplished by first calculating $|\nabla\vec{I}|^2 \cos 2\phi$ and $|\nabla\vec{I}|^2 \sin 2\phi$, locally Gaussian averaging each of these two fields independently, and then using these two fields to calculate θ.

Gaussian averaging obtains a well-defined director value even in regions where the gradient is not well-defined locally, such as in the middle of a cylinder. The order parameter of each director angle is averaged with the values of its neighbors over a square area with sides of size 2λ. A Gaussian average is performed for each point by weighting its neighbors' intensities with a Gaussian profile (where σ of the Gaussian profile is typically equal to λ) of descending weighting value, normalized such that the sum of the weights over the entire square equals 1. Without Gaussian averaging, a periodicity of half the microdomain spacing is strongly represented in the director field, due to the poorly defined gradient orientation at the troughs and crests of the intensity field. Note that by weighting the director fields by $|\nabla\vec{I}|^2$ these poorly defined regions contribute little after the Gaussian average.

As a final step, the director angle θ is obtained by calculating the arctangent of the ratio of the two fields at each position (eq 3), and this angle is used to obtain the order parameter field using eq 1. Note that this last step discards the local magnitude of the Gaussian-averaged director field while preserving and enhancing the local director.

$$\theta = \arctan\left(\frac{|\nabla\vec{I}|^2 \sin(2\phi)}{|\nabla\vec{I}|^2 \cos(2\phi)}\right) \tag{3}$$

e. Correlation Calculation. To ascertain the correlation length, we first calculate the correlation function of the order parameter. Since we have chosen the image dimensions to include many grains, the Fourier transform of the image intensity $I(x,y)$ produces the familiar powder pattern seen by small-angle X-ray or neutron scattering from polycrystalline samples. The average value of the nematic order parameter is close to zero. When we calculate the orientational correlation, therefore, we sum the correlation pairs of the nematic order parameter along all directions for each correlation distance r.

Because of the Gaussian averaging that is performed, the local value of the order parameter is a smoothly varying function of position. Therefore, it was observed to be unnecessary to calculate the correlation of the order parameter associated with each position; rather, we sample only every 10th director angle (which is approximately one director angle per distance λ) in the x and y directions in the autocorrelation of the order parameter. This process does not significantly sacrifice accuracy since we have averaged the director angle over a square region of breadth 2λ. This greatly reduces computation time while not significantly affecting the accuracy of our calculation. Thus, we define the orientational correlation function:

$$g_2(r) = \langle\psi(0)\,\psi^*(r)\rangle \tag{4}$$

The correlation length is estimated from the position r where the $g_2(r)$ decays to e^{-1}. An example of two correlation functions is shown in Figure 5. Note that any fluctuations of $g_2(r)$ about zero for large r result from the noise associated with a paucity of correlation pairs at large separation distances.

C. Study of SBS ξ over Wide Range of Temperatures. Though the two images of Figure 3 suggest that the bare substrate can pin the copolymer chains, these images do not tell us whether we have obtained the equilibrium configuration or whether this observation is highly temperature dependent. Therefore, SBS samples

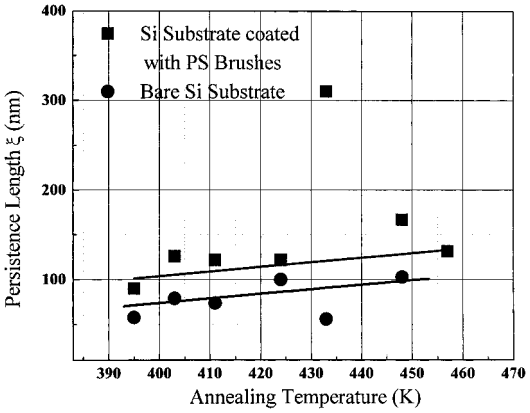

Figure 7. Persistence length ξ for SBS films were annealed from 395 to 456 K on both bare silicon substrates and PS brush-coated substrates for 12 h periods. Though there is a substantial amount of scatter, the data consistently show that ξ is larger for SBS films decoupled from the substrate by PS brushes.

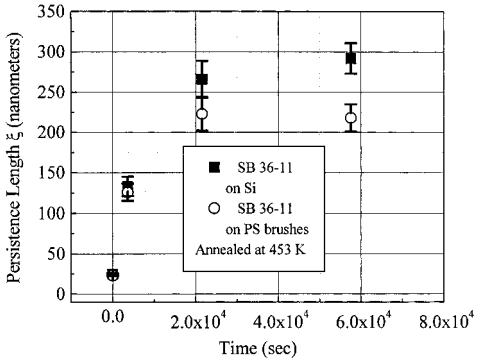

Figure 8. Comparison of SB 36/11 annealed on silicon substrates and annealed on a PS brush-coated substrate. Though ξ is similar for both substrates, it is slightly higher at late times for microdomains on the bare Si substrates.

were annealed on both bare silicon and PS brush-coated silicon substrates for 12 h at temperatures ranging from 395 to 456 K. The correlation (or persistence) length was calculated for each of these samples and is shown in Figure 7. Error bars for each sample were calculated from the variance in correlation lengths as measured from at least four SEM images and are approximately the size of the data points. For every annealing temperature, a significantly higher value of the microdomain orientational correlation length is measured for microdomains on PS brush-coated wafers than on bare wafers. There is much scatter in these data, so solid lines have been added as a guide to the eye. In particular, the samples annealed at 433 K are the most extreme example of this inconsistency; however, they are consistent with the persistence length being higher on PS-coated substrates. We note that this inconsistency was seen more in the commercial SBS than in the polymers synthesized in-house. In addition, while samples were prepared together for a given annealing temperature, samples sets for each annealing temperature were fabricated on different days and hence under slightly different conditions, which may be the origin of the scatter in Figure 7. However, ξ is consistently higher on the PS brush-coated wafers for samples at each annealing temperature, suggesting that the PS brushes mitigate substrate pinning.

Since the energy density of microdomains is directly proportional to $1/R_c^2$, microdomains that are closer to their equilibrium configuration will exhibit a larger radius of curvature and a larger value of ξ.[35] We suggest that displacing the SBS chains from the potentially pinning influence of the substrate allows the cylindrical microdomains to develop into a configuration closer to their equilibrium pattern. Since the correlation length is only weakly temperature sensitive, we suggest that the microdomain pattern is not dominated by temperature-dependent barriers to further growth, like those shown by Balsara and co-workers,[4−7] but rather this may imply that ξ is primarily limited by substrate pinning.

We note that while thick polymer sublayers (e.g., PMMA) can also be used to decouple subsequently applied copolymer layers from the substrate, PS brushes offer the ability to make ultrathin (∼5 nm) buffer layers. For nanolithographic templates, it is important to separate the copolymer microdomains from the substrate as narrowly as is possible to avoid widening the pattern features during etching.[9]

3. PS-Rich Copolymers on Substrates. To study the effect of the substrate on the correlation length of microdomains in PS-rich copolymers, we prepared two sets of substrates: one with a bare silicon wafer and one with a layer of PS brushes. On these samples we spin-coated a monolayer of SB 36/11 cylinders. To satisfy the wetting constraints of the two substrates, the monolayer was 50 nm thick on the bare silicon substrate and 35 nm thick on the PS brush-coated substrate. We annealed these samples simultaneously at 453 K. Samples were stained and imaged as previously described, including etching away the PB free surface wetting layer to enhance the contrast as seen by electron microscopy.

We found that the two substrates produced quite similar correlation lengths for the two microdomain patterns (Figure 8), but ξ was slightly lower on the PS brush-coated wafers. For both samples, ξ rapidly increases initially at early times and then appears to saturate at around 250 nm for longer times. Annealing the sample for longer times at this high temperature induced degradation, as evidenced by randomly distributed disordered spherical microdomains. Annealing for even longer times degrades the carbon−carbon double bonds such that selective staining is no longer possible. We examined the dependence of the periodicity on the annealing time for both SB 36/11 data sets of Figure 8. The average periodicity was calculated from the radius of the powder pattern in the Fourier transform of the microdomain patterns. We found that the periodicity remained at a constant value of 23 ± 0.5 nm regardless of the value of ξ. This indicates that the annealing of the microdomain pattern is occurring well after the chains, and hence microdomains, have adopted their equilibrium size.

The slightly lower value of ξ for SB 36/11 on surfaces without PS brushes at late times suggests that the interfacial wetting layers (thereby self-lubricating) of SB 36/11 decouple the microdomains from the substrate more effectively than the PS brushes. This may be because the thicker (∼15 nm) self-lubricating layers of SB 36/11 are a better buffer layer than the PS brushes (∼5 nm). The PS brushes that are attached to the substrate in Figure 1b act like the PB wetting layer on the substrate for the cylinders seen in Figure 1a. Note that in both cases the polymer chains that form the actual PB microdomains are not in direct contact with

the inorganic substrate, minimizing pinning of the polymer chains. We are currently investigating the time and temperature dependence to determine the origin of this saturation of ξ, which appears to be related to a Peierls-like energy barrier associated with moving defects through the copolymer layers.

Conclusions

We have employed a recently developed imaging technique to study the correlation length of copolymer microdomains on several substrates. By attaching a layer of PS brushes to the silicon substrate (Figure 1), we add a buffer layer which also modifies the affinity of the copolymer blocks for the substrate. After modification of the substrate, thin films of SBS form discrete thicknesses that are commensurate with the number of cylinder layers (Figure 3). Without this modification, the SBS films are pinned to the substrate, as evidenced by a lack of terracing and a correlation length where ξ is not much larger than λ. We demonstrate that this short correlation length of copolymer layers without self-lubricating layers can be overcome (Figure 7) by placing a thin buffer layer of PS brushes between the substrate and the copolymer layers. The correlation length of copolymers with self-lubricating layers (SB 36/11), however, is slightly less sensitive to the substrate than copolymer layers without self-lubricating layers (Figure 8), and one finds similar or higher correlation lengths without PS brushes.

Acknowledgment. We gratefully acknowledge the assistance of Srinivas Manne and Tu Lee with initial investigations of SBS. This work would not have been possible without the advice and efforts of Michael J. Valenti of the Advanced Technology Centre for Photonic and Optoelectronic Materials (ATC/POEM) of Princeton University regarding wafer cleaning. We gratefully acknowledge the staff of the Cornell Nanofabrication Facility for their advice and efforts. This work was supported by the National Science Foundation through the Princeton Center for Complex Materials (DMR-9400362 and DMR-9809483), DMR-9802468, and the Materials Research Science and Engineering Center at the University of Massachusetts (DMR-9400488).

References and Notes

(1) Bates, F. S.; Fredrickson, G. H. *Annu. Rev. Phys. Chem.* **1990**, *41*, 525.
(2) Henkee, C. S.; Thomas, E. L.; Fetters, L. J. *J. Mater. Sci.* **1988**, *23*, 1685.
(3) Newstein, M. C.; Garetz, B. A.; Balsara, N. P.; Chang, M. Y.; Dai, H. J. *Macromolecules* **1998**, *31*, 64.
(4) Dai, H. J.; Balsara, N. P.; Garetz, B. A.; Newstein, M. C. *Phys. Rev. Lett.* **1996**, *77*, 3677.
(5) Garetz, B. A.; Balsara, N. P.; Dai, H. J.; Wang, Z.; Newstein, M. C.; Majumdar, B. *Macromolecules* **1996**, *29*, 4675.
(6) Balsara, N. P.; Garetz, B. A.; Dai, H. J. *Macromolecules* **1992**, *25*, 6072.
(7) Newstein, M. C.; Garetz, B. A.; Dai, H. J.; Balsara, N. P. *Macromolecules* **1995**, *28*, 4587.
(8) Park, M.; Harrison, C.; Chaikin, P. M.; Register, R. A.; Adamson, D. H. *Science* **1997**, *29*, 4494.
(9) Harrison, C.; Park, M.; Chaikin, P. M.; Register, R. A.; Adamson, D. H. *J. Vac. Sci. Technol. B* **1998**, *16*, 544.
(10) Annis, B. K.; Schwark, D. W.; Reffner, J. R.; Thomas, E. L.; Wunderlich, B. *Makromol. Chem.* **1992**, *193*, 2589.
(11) Chen, J. T.; Thomas, E. L. *J. Mater. Sci.* **1996**, *31*, 2531.
(12) Hahm, J.; Lopes, W. A.; Jaeger, H. M.; Sibener, S. J. *J. Chem. Phys.* **1998**, *109*, 10111.
(13) Harrison, C.; Park, M.; Chaikin, P. M.; Register, R. A.; Adamson, D. H.; Yao, N. *Polymer* **1998**, *30*, 2733.
(14) Harrison, C.; Park, M.; Chaikin, P. M.; Register, R. A.; Adamson, D. H. *Macromolecules* **1998**, *31*, 2185.
(15) Huang, E.; Russell, T. P.; Harrison, C.; Chaikin, P. M.; Register, R. A.; Hawker, C. J.; Mays, J. *Macromolecules* **1998**, *31*, 7641.
(16) Ahagon, A.; Gent, A. N. *J. Polym. Sci., Polym. Phys. Ed.* **1975**, *13*, 1285.
(17) Jones, R. A. L.; Norton, L. J.; Shull, K. R.; Kramer, E. J. *Macromolecules* **1992**, *25*, 2539.
(18) Mansky, P.; Chaikin, P. M.; Thomas, E. *J. Mater. Sci.* **1995**, *30*, 1987.
(19) Morton, M.; Fetters, L. J. *Rubber Chem. Technol.* **1975**, *48*, 359.
(20) Krause, S.; Lu, Z.-h; Iskander, M. *Macromolecules* **1982**, *15*, 1076.
(21) Morrison, F.; Winter, H. H. *Macromolecules* **1989**, *22*, 3533.
(22) Tung, L. H. *Fractionation of Synthetic Polymers: Principles and Practices*, M. Dekker: New York, 1977.
(23) Mansky, P.; Liu, Y.; Huang, E.; Russell, T. P.; Hawker, C. *Science* **1997**, *275*, 1458.
(24) Hawker, C. J. *J. Am. Chem. Soc.* **1994**, *116*, 11314.
(25) Hawker, C. J.; Barclay, G. G.; Orellana, A.; Dao, J.; Devonport, W. *Macromolecules* **1996**, *29*, 5245.
(26) Hawker, C. J.; Elce, E.; Dao, J.; Volksen, W.; Russell, T. P.; Barclay, G. G. *Macromolecules* **1996**, *29*, 2686.
(27) van Roosmalen, A. J.; Baggerman, J. A. G.; Brader, S. J. H. *Dry Etching for VLSI;* Plenum Press: New York, 1991.
(28) Park, M.; Harrison, C.; Chaikin, P. M.; Register, R. A.; Adamson, D. H.; Yao, N. *Mater. Res. Soc. Symp. Proc.* **1997**, *461*, 179.
(29) Coulon, G.; Ausserre, D.; Russell, T. P. *J. Phys.* (*Paris*) **1990**, *51*, 777.
(30) Lee, T.; Yao, N.; Aksay, I. A. *Langmuir* **1997**, *13*, 3866.
(31) van Dijk, M. A.; van den Berg, R. *Macromolecules* **1995**, *28*, 6773.
(32) Egolf, D. A.; Melnikov, I. V.; Bodenschatz, E. *Phys. Rev. Lett.* **1998**, *80*, 3228.
(33) Meyer, R. B.; Lubensky, T. C. *Phys. Rev. A* **1976**, *14*, 2307.
(34) Chandrasekhar, S. *Liquid Crystals,* 2nd ed.; Cambridge University Press: New York, 1992.
(35) Amundson, K.; Helfand, E. *Macromolecules* **1993**, *26*, 1324.
(36) For a good review of two-dimensional smectics, see for example: Toner, J.; Nelson, D. R. *Phys. Rev. B* **1980**, *23*, 316.
(37) Harrison, C. Ph.D. Thesis, Princeton University, 1999.

MA991551G